Dual-season comparison of OBIA and pixel-based approaches for coastal wetland classification

Comparação de abordagens baseadas em objetos (OBIA) e em pixels em duas estações para a classificação de áreas úmidas costeiras

João Paulo Delapasse Simioni[1] ⦿ & Laurindo Antonio Guasselli[1] ⦿

[1]Universidade Federal do Rio Grande do Sul, Porto Alegre, RS, Brasil
E-mails: geojoaopaulo@gmail.com (JPDS), laurindo.guasselli@ufrgs.br (LAG)

ABSTRACT

Mapping and classifying Coastal Wetlands is important for their conservation. The study aimed to apply Object-Based Image Analysis (OBIA) and pixel-based approaches to answer the questions: (1) which approach is more accurate for classifying Wetlands; (2) Sentinel 1A images improve the classification of Wetlands compared to Sentinel 2A; (3) dual-station sorting has greater potential for sorting Wetlands compared to single-station sorting. We used Sentinel 1 and 2 in single and double seasons (winter and summer) to classify a coastal UA in Rio Grande do Sul. The results show OBIA with greater potential, with accuracy greater than 80%. Sentinel 2 shows higher ranking importance compared to Sentinel 1. Dual season OBIA increased kappa by up to 7% compared to single season. Furthermore, the pixel-based dual season had lower kappa than the OBIA single season. We conclude that OBIA, even at a single station, has greater potential to map coastal AUs.

Keywords: Machine learning; Coastal wetlands; São Gonçalo channel.

RESUMO

Mapear e classificar Áreas Úmidas Costeiras é importante para a sua conservação. Este estudo teve como objetivo aplicar Análise de Imagens Baseada em Objetos (OBIA) e abordagens baseadas em pixels para responder às questões: (1) qual abordagem é mais precisa para classificar Áreas Úmidas; (2) as imagens do Sentinel 1A são melhores para classificação das Áreas Úmidas em comparação com o Sentinel 2A; (3) a classificação em estação dupla tem maior potencial para classificação de Áreas Úmidas em comparação com a classificação em estação única. Utilizamos Sentinel 1 e 2 em estações simples e duplas (inverno e verão) para classificar uma Área Úmida costeira no Rio Grande do Sul. Os resultados mostram OBIA com maior potencial, com precisão superior a 80%. O Sentinel 2 apresentou maior importância na classificação em comparação com o Sentinel 1. O OBIA de estação dupla aumentou o kappa em até 7% em comparação com a estação única. Além disso, a estação dupla baseada em pixels teve kappa menor do que a estação única do OBIA. Concluímos que o OBIA, mesmo em uma única estação, tem maior potencial para mapear Áreas Úmidas costeiras.

Palavras-chave: Aprendizado de máquina; Áreas úmidas costeiras; Canal São Gonçalo.

INTRODUCTION

Wetlands play a key role in hydrological and biogeochemical cycles and are home to much of the world's biodiversity (Kandus et al., 2018; Sinthumule, 2021). They provide ecosystem services (Mitsch & Gosselink, 2015; Li et al., 2019), such as microclimate regulation (Şimşek & Ödül, 2018), carbon sequestration (Zhang et al., 2023), flood mitigation (Vanderhoof et al., 2016; Rojas et al., 2022), climate change mitigation (Ramachandran et al., 2023).

South American subtropical wetlands vary according to morphology, structure, area, vegetation patterns and duration/extent of flooding (Costa et al., 2016; Terra et al., 2022). The Pantanal and the floodplains of the Paraná-Paraguay rivers stand out (Kandus et al., 2018), where the interior wetlands are fed by the seasonal overflow of rivers, groundwater and local rainfall (Junk et al., 2014; Lázaro et al., 2020).

Despite their importance, SASW suffer impacts such as conversion to agricultural and urban land (Simioni et al., 2019). However, mapping and classifying wetlands are not simple tasks. Researchers who develop methodologies to map and classify these environments must overcome challenges, such as lack of financial resources, difficult access to wetlands (Cunha et al., 2023; Rapinel et al., 2023).

Optical remote sensing is an important tool for mapping and classifying wetlands (Guo et al., 2017). The best spectral and radiometric resolutions of Landsat 8 OLI of Sentinel 2 MSI have enabled better accuracy to map and classify these areas. One of the main problems that involves optical sensors is the spectral similarity of wetland vegetation, mainly due to the presence of water in the vegetation (Ruiz et al., 2021; Tran et al., 2022).

One way to overcome these issues is the use of active Synthetic Aperture Radar (SAR) sensors. Remote sensing by SAR has great potential as a complement to optical images (Jahncke et al., 2018; Mohammadimanesh et al., 2018). Their main advantages are penetration through clouds, data acquisition during the day or night and, in the case of vegetation, access to information from the entire canopy and not just the first leaves layer (Wang et al., 2018; Tian et al., 2023).

The development of new classification techniques can complement those based on pixels (Mahdianpari et al., 2017). Object-Based Image Analysis (OBIA) segments images into "objects" which are groups of pixels representing points on the ground, entities or their primitive elements that can be classified into categories by unsupervised, supervised, or based on rules of analysis algorithms (Blaschke et al., 2014). For Dronova (2015), OBIA has advantages over the pixel-based approach, such as the possibility of incorporating shape, texture and relevant contextual variables of the object in the classification, in addition to the spectral values of the layers of the input image and the objects smoothing, which can reduce salt and pepper noise and increase classification accuracy (Prentice et al., 2022).

The literature shows better OBIA accuracy over the pixel-based approach to classify wetland types (Kaplan & Avdan, 2019). For The OBIA approach improved overall accuracy in classifying vegetation in wetlands compared to the pixel-based approach (Fu et al., 2017; Berhane et al., 2018; Zheng et al., 2022).

Pande-Chhetri et al. (2017) used images from unmanned aerial vehicles and an OBIA approach, and observed higher accuracy than that observed outside the pixel-based approach.

Most of the studies use only one image date to map and classify wetlands. However, the landscape of coastal wetlands is dynamic, showing strong seasonal fluctuations in water levels and growth and senescence of vegetation (Daí et al., 2019; Bergamo et al., 2022). Both backscatter in SAR images and reflectance in optical images are strongly affected by these seasonal changes (Furtado et al., 2016; Prudente et al., 2022), justifying the importance of dual-season analysis.

The Brazilian territory is composed of 20% wetlands, with emphasis on the Amazonian floodplain and the Pantanal (Junk et al., 2014; Milien et al., 2023). Unlike the North and Midwest regions of Brazil, which are characterized by large wetlands, the South of Brazil has a complex of small wetlands, generally located along river floodplains and coastal areas. Due to their size (generally less than 1,000 ha) (Maltchik et al., 2004), the wetlands of southern Brazil have long been ignored by federal and state governments, lacking policies aimed at protecting and conserving these small environments, but complex. The Federal Government's Pró-Várzea program in 1940, for example, encouraged the drainage of these ecosystems for the development of agriculture, responsible for the destruction of more than half of the wetlands in Rio Grande do Sul (Burger, 2000).

The São Gonçalo Channel (CGS) is a subtropical complex of coastal wetlands in southern Brazil. Since the 1940s, advances in rice cultivation areas have converted large areas of swamps and wet meadows into cultivable areas, with enormous damage to the environment and biodiversity (Food and Agriculture Organization, 1972).

Based on the considerations, this study aims to apply the OBIA and pixel-based approaches and answer the following questions: (1) which approach is more accurate to classify subtropical coastal wetlands; (2) do Sentinel 1A C-band dual-pol SAR images improve the classification of subtropical coastal wetlands when compared to Sentinel 2A optical images; and (3) does the dual-season classification have greater potential for classifying subtropical coastal wetlands compared to the single-season classification.

METHODS

Study area

The São Gonçalo Chanel (SGC) is located in the southern region of the coastal plain of the state of Rio Grande Sul, Brazil (31°47'S; 52°14'O and 32°12'S;52°40'O) (Figure 1) (Albertoni et al., 2017). The SGC is an important wetland that connects the two largest lagoons in Rio Grande do Sul (Patos and Mirim). The channel has a winding course approximately 74 km long and up to 10 m deep.

The SGC is part of the geomorphological domain of sedimentary deposits, divided into two geomorphological regions: i) external coastal plain (marine influence) and internal coastal plain (influence of the Patos/Mirim fluvial-lacustrine system) (Radam Brasil, 1986; Simon & Silva, 2015). The geology is characterized by peatlands deposits, floodplain deposits and alluvial deposits (Serviço Geológico do Brasil, 2004).
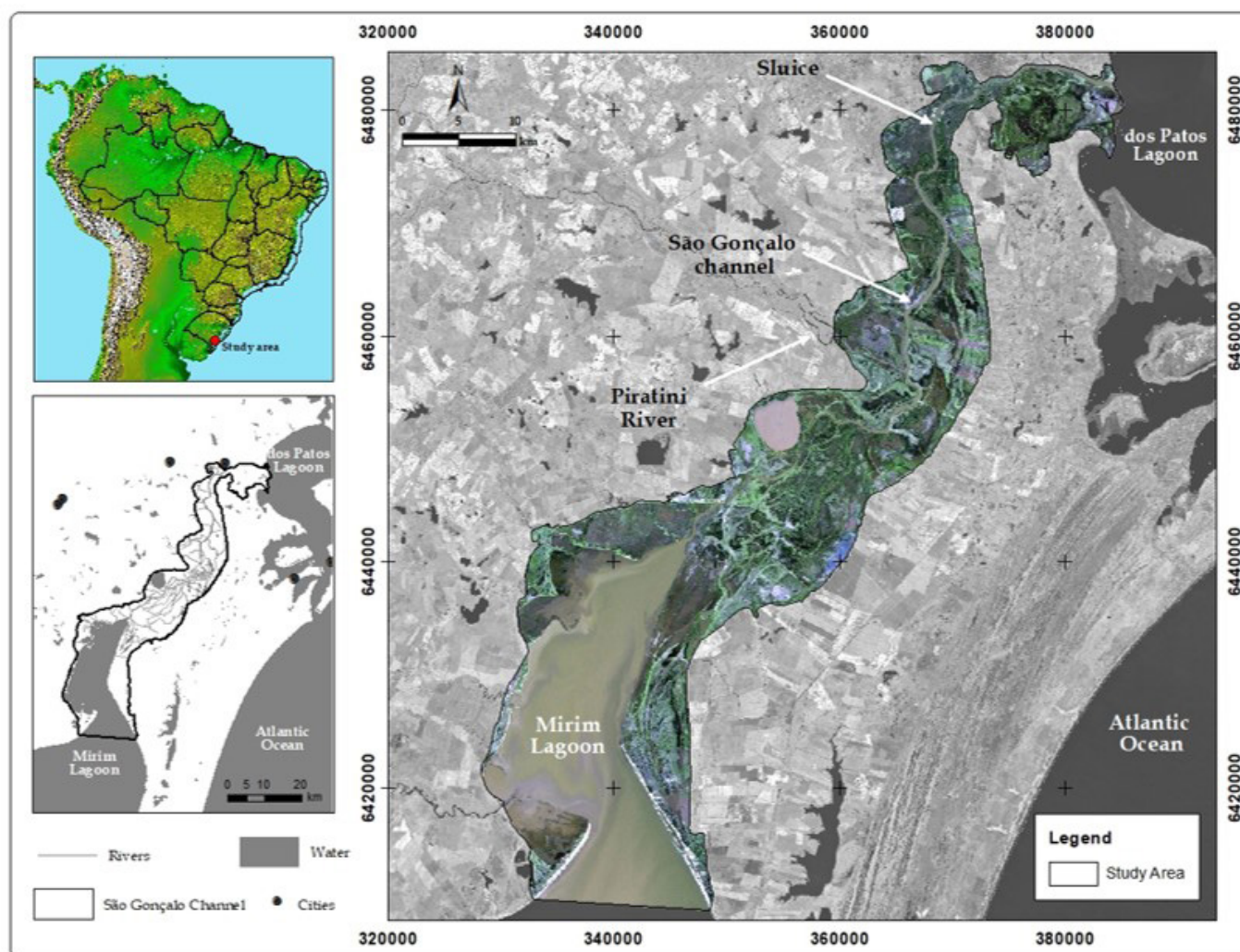
Figure 1. Location of São Gonçalo channel, southern region of coastal plain, Rio Grande do Sul.

According to the Koppen classification, the climate in the SGC is *Cfa* (subtropical with hot summers) (Mengue et al., 2020). The average annual rainfall ranges between 1,300 and 1,600 mm (Instituto Nacional de Meteorologia, 2020). According to Collischonn (2016) in Pelotas, the climate is controlled mainly by the action of the Polar (mP) and Tropical Atlantic (mTa) masses. There are hot summers (22.9°C on average) and cool winters (13.2°C on average). Frontal systems are active at all times of the year and regulate both the rhythm of precipitation (rains are generally pre-frontal, frontal or post-frontal) and winds (Figure 2).

In 1970, Brazil and Uruguay, in partnership with the Food and Agriculture Organization (1972), carried out studies on regional agricultural development. A lock was built to contain the entry of salt water from the Atlantic Ocean, through Lagoa dos Patos towards Lagoa Mirim, helping to simplify regional agricultural production (Burns, 2010). According to Instituto Rio Grandense do Arroz (2019), the south of Rio Grande do Sul has 152,073 ha of rice planted area, representing ~16% of the total rice cultivated area in the state.

The natural flow of the SGC runs south (Lagoa Mirim) to North (Lagoa dos Patos). In periods of high tide or low rainfall,
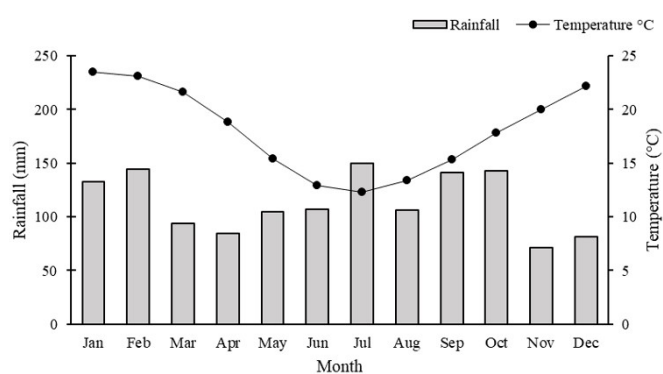

Figure 2. Average monthly rainfall and air temperature in São Gonçalo channel.
Source: Capão do Leão (Pelotas) INMET Meteorological Station (-31,802500, -52,407222, 13m).

the flow of the channel is reversed and the lock is closed to prevent the entry of brackish water into the Mirim lagoon (Burns, 2010). Figure 3 shows a stretch of the lock in the normal period (Figure 3a) with a flood pulse in September 2002 (Figure 3b).

The vegetation of the SGC is mainly composed of marshes, trees and shrubby and wet meadows (Table 1). The sluice, located 17 km from Patos lagoon, blocks salt water from the ocean and regulates the flow of the channel, influences the dynamics of wetlands (Duarte, 2013) and, consequently, the distribution of species (Burns, 2010). This fact allows the development of two types of marshes: salt marshes (between Patos lagoon and the sluice) and freshwater marshes (between the sluice and Mirim lagoon).

Fieldwork and samples

Training samples were obtained from field work carried out carried out between February 25 and 27, 2019 (summer in South hemisphere) and August 5 and 7, 2019 (winter in South hemisphere). And also, based on visual interpretation of two images from the RapidEye satellite (Planet) with 5 m of spatial resolution.

50 sampling points were defined using georeferenced photographs throughout the SGC, and observations of vegetation features, the influence of water and topographic gradients were recorded. Plant communities were classified into 3 main vegetation types (swamps, trees and shrubs, and wet meadows). Table 1 describes the species, based on the hierarchical level of dominant plant species in wetlands, according to Irgang et al. (1996), Maltchik et al. (2004).

In each location, the type of vegetation covered a homogeneous area of at least 1,000 m² x 1,000 m². We also recorded samples at 5 sites with open water (shallow lakes and SGC) and 5 sites with the presence of sand dunes and bare soil. For the visual interpretation, a regular grid with 1,330 points with 1,000 m equidistances was generated and each point was assigned to the corresponding class. A visual interpretation was then performed in a regular grid with 1,330 points equidistant from 1,000 m, and each class was assigned to each point.

The validation samples consisted of 550 points generated at random order, considering the same chance of selection for all geographic objects. The regular grid of the training samples and the validation samples were the same for the two stations. The accuracy of the classification was measured by the following indexes: (1) coefficient kappa; (2) correct proportion (CP) (Pontius & Millones, 2011); (3) producer's accuracy (PA); and (4) user's accuracy (UA) (Story & Congalton, 1986).

Sentinel images

Sentinel 1 and 2 images (Table 2) were used to classify wetlands in the SGC. The SAR images of the Sentinel 1A C-band were acquired in Ground Range Detected (GRD) format, with 10 m spatial resolution and level 1 pre-processing in the VV and VH polarizations.
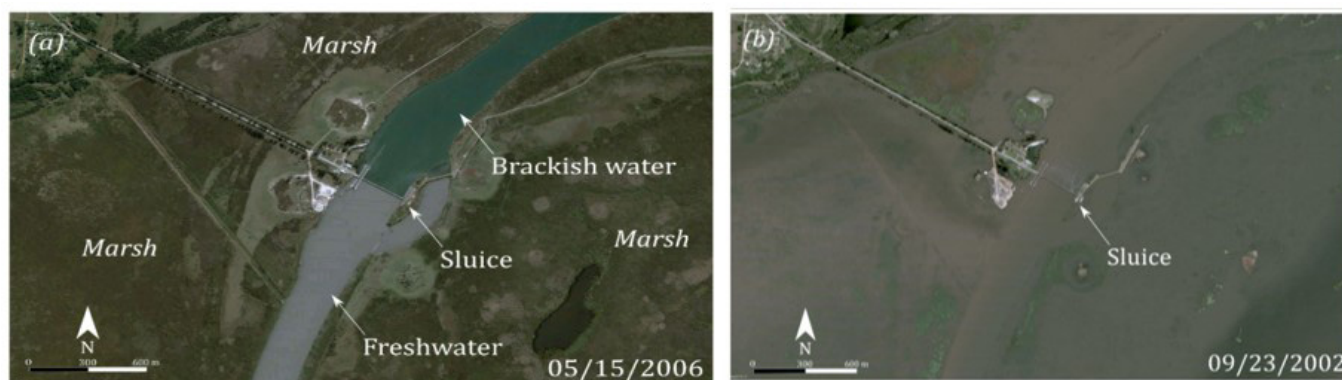
Figure 3. Sluice in São Gonçalo channel: (a) separation between fresh and brackish water; (b) flood pulse event.
Source: Google Earth Pro.

Table 1. Dominant species in São Gonçalo Channel.

Class	Dominant Species/ typology
Marshes	*Scirpus sp., Cyperus sp., Zizaniopsis sp., Eryngium pandanifolium, Juncus L. Eichhornia crassipes, Eichhornea azurea, Salvinia auriculata, Hydrochleis nymphoides, Leersia sp., Cabomba australis, Leersia sp., Pontederia lanceolata, Nymphoides sp., Hygrophila sp., Polygonum spp., Myriophillum brasiliensis.*
Tree and shrubby	*Cephalanthus sp., Mimosa sp. Calliandra sp., Erythrina sp.*
Wet Meadow	*Erianthus sp., Andropogon bicornis, Sida sp., Mimosa bimucronata, Panicum prionitis and grasses*

Source: Irgang et al. (1996), Maltchik et al. (2004).

Table 2. Sentinel images used in the study.

	Winter	Summer	Resolution	Relative Orbit	Product type
Optical	08/06/2019	02/27/2019	10 m	081	S2MSI1C
SAR	09/06/2019	02/25/2019	10 m	024	GRD

In the Sentinel Application Platform (SNAP) software, the following procedures were applied: radiometric calibration, speackle filter and geometric correction. We used the SNAP software for the image digital processing according to the flowchart presented in (Figure 3). First, the radiometric calibration was applied. The radiometric calibration is necessary to compare the SAR images, obtained at different dates/times. In addition, the radiometric calibration of the SAR images is required to provide images in which pixel values can be directly related to the scene radar backscatter (Clevers, 2015). Second, the speckle filtering Refined Lee 5 x 5 used in (Furtado et al., 2016) was applied to reduce the image noise and to correct the geometry using the geolocation grid tool.

Optical images of Sentinel 2A Multispectral Instrument (MSI) with 1C pre-processing level, were orthorectified and converted to reflectance at the top of the atmosphere. Sentinel 2 image was pre-processed to 2A level using the *Sen2Cor* tool (Sentinel Application Platform - SNAP) in order to remove the atmospheric effects and to convert the pixel values for surface reflectance (Chatziantoniou et al., 2017). Bands 1, 9 and 10 were removed because they are collect specific information regarding coastal aerosol, water vapor and cirrus type clouds radiations, respectively.

Pixel-based approach

The pixel-based classification consists of analyzing the individual pixels of the image, based on the spectral information contained in each band. A pixel-based approach is a traditional classification approach, since the pixel is the fundamental spatial unit of a satellite image (Abdikan et al., 2016).

For the pixel-based classification, the reflectance values of the bands B2, B3, B4, B5, B6, B7, B8, B8A, B11 and B12 were extracted from the Sentinel 2A and the backscatter values of the VV and VH channels Sentinel 1A satellite, for each training sample. The process was performed for both the Summer and the Winter images.

Object-based image approach

Features and segmentation

For segmentation, the following bands were used: B2, B3, B4, B5, B6, B7, B8, B8A, B11 and B12 from the Sentinel 2A MSI satellite and the VV and VH polarizations from the Sentinel 1A satellite.

From the fusion by Principal Component Analysis (PCA), using the System for Automated Geoscientific Analyzes (SAGA-GIS) software, bands B5, B6, B7, B8A, B11 and B12 with a spatial resolution of 20 m were converted to 10 m. For fusion, a panchromatic image was generated using the average value of bands with spatial resolutions of 10 m (B2, B3, B4 and B8) (Kaplan & Avdan, 2018).

Different segments for Winter, Summer and dual-season were created in QGIS 3.8 software. For segmentation, we used the region-growth algorithm (Happ et al., 2013). The region-growth segmentation brings together adjacent pixels that meet heterogeneity criteria.

The regions of the image are grouped or divided depending on whether the pixels have similar characteristics in terms of color, texture or shape.

The region-growth algorithm is controlled by the similarity threshold (ST). Values from 0 to 1 varying by 0.250 were tested. High ST values mean higher freedom for growth of the regions (geographic objects) and vice-versa. In addition, we evaluated the scale, which determines the minimum size of the geographic objects. Low scale values mean smaller geographic-objects generated by the segmentation. We tested scale values between 200 and 600, varying by 200.

From the segmentation, the statistics of the features, the average and the standard deviation of the segmented polygons for each of the 12 features of the single-season and 24 features for the dual-season were extracted (Ruiz, 2018).

Classification

The classifications were performed using the Decision Tree (DT) method with the Classification and Regression Trees (CART) algorithm. The CART method uses the binary recursive partitioning analysis for class discrimination, in which each parent node is divided into two child nodes (Breiman et al., 1984; Lawrence & Wright, 2001). The process is repeated by treating each child node as a parent node. When data from a node cannot be divided into additional nodes, it is called the terminal node. Once the first terminal node has been created, the algorithm repeats the procedure for each data set until all data are categorized as terminal nodes (Waheed et al., 2006).

The tree complexity can be controlled by its depth and child nodes sample numbers. The following sample values were evaluated for depth (5, 8, 10, 15, 20, 25, 30, 35). For the minimum number of samples (MNS) in child node: 5, 10, 20, 40, 60, 80 and 100. In addition, the Gini index (Gini, 1912) was used as the impurity measure of tree branches.

The Gini index measures the data heterogeneity degree, by searching the largest category in the dataset (e.g. marshes) and isolating it from the other categories (Waheed et al., 2006). Equation 1 gives Gini index in a given node:

$$Gini = 1 - \sum_{i=1}^{c} p_i^2 \qquad (1)$$

Where: p_i is each class relative frequency in each node; c is the class number. In this study, we defined four classes.

When the Gini index is zero, the node is pure. However, when the Gini index approaches one, the node is impure and increases the number of classes evenly distributed on this node. In the CART method, the Gini index isolates in a branch the records that represent the most frequent class (Breiman et al., 1984).

RESULTS

The comparison between the results obtained by the OBIA and Pixel approaches showed significant differences in kappa between the segmentation parameters (Figure 4). In the OBIA approach, kappa values varied according to similarity limits, scale (size of geographic objects), as well as seasonality (Winter and Summer).

In winter, kappa varied between 0.59 and 0.80. The largest kappas were found in the segmentation with a scale parameter of 200, and it shows that the size of the geographic objects has a greater influence on the kappa values than the similarity threshold. In summer, kappa varied between 0.57 and 0.79. The highest values were found in the 400 scale parameter and show the importance of testing with different parameters in segmentation.

In addition to the segmentation parameters, the CART parameters (number of internal node samples and tree depth) can also influence the kappa values (Table 3). The minimum number of samples to divide the internal nodes varied between 3 and 10, while the maximum depth of the DT (length of the longest path, from the root to the leaf of the DT) varied between 25 and 30.

In the decision trees the DT of the OBIA-based approach for the summer presented the largest number of internal nodes, with 25. The lowest DT was the pixel-based approach of the winter, with 9 internal nodes, the parent node was the band B12 (SWIR). DT based on pixel for the summer presented 15 internal nodes and, as in the OBIA-approach, the parent node of DT for the summer was the band B8.

The SGC classification showed similar patterns for the occurrence of marshes, trees and shrubs and wet meadow (Figure 5). The main difference between OBIA and pixel approaches was the amount of noise present in the classifications. OBIA images have the ability to incorporate objects into the classification, reducing the noise.

The marsh areas are mainly observed in three sectors of the SGC: in the north, central area (near Formosa lagoon) and in the south (near Mirim lagoon). Marsh is the vegetation class with the highest occurrence in the SGC in both approaches. This vegetation is mainly composed of *Cyperaceaes* of the genus *Scirpus sp.*, characterized by dense vegetation, varying between 1.5 and 2.5 m above the water layer (Figure 6a). In the field, we verified that *Scirpus sp.* presents the same distribution pattern in the areas before and after the sluice.

The areas of trees and shrubs are restricted to fragments near the mouth of the Piratini River, north of Formosa lagoon.

The wet meadow areas, commonly found in the Pampa biome, are primarily composed of grasses. These grasses show differences in the toral area between the winter and summer seasons, due to the water level fluctuations in the SGC (Figure 6b). In the winter, both approaches presented smaller areas of wet meadow, compared to the summer. This can be explained by the higher rainfall in the winter months when wet meadow areas tend to be flooded (Figure 6b).

In Rio Grande do Sul, rice cultivation takes place between October and March. The germination of lost grains during the harvest is common, which may explain the occurrence of rice crops in winter. In the summer image, the period corresponding to the end of tillering in rice cultivation, the OBIA classification estimated more than half of the rice areas when compared to the pixel-based approach (Table 4).

The highest overall accuracy in initialization times according to the classification confusion matrices was found in the OBIA-based approach. For the winter, the overall accuracy reached 0.83 and the kappa coefficient of 0.80. The producer and the user's accuracy were also calculated for the four classifications.

The biggest OBIA commission errors for the winter were in the wet meadow class (0.62), with the highest confusions attributed to bare soil and rice crop. The major omission errors for the OBIA approach (winter and summer) were found in the Bare Soil class (0.52 and 0.40, respectively).
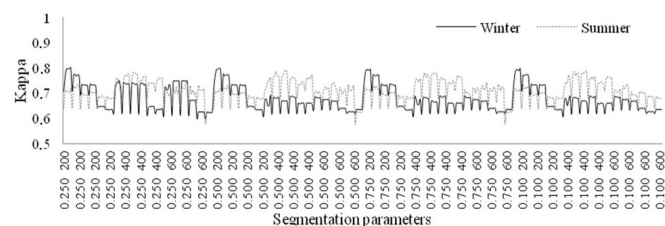

Figure 4. Relationship between segmentation parameters (similarity threshold_minimum number of cells) and kappa.

Table 3. Best parameters of the Decision Tree.

	Minimun Number Samples	Depth	Kappa
OBIA (winter)	10	30	0.80
OBIA (summer)	15	25	0.79
Pixel (winter)	5	30	0.68
Pixel (summer)	3	30	0.62

Table 4. Comparison of class areas (km² and %) with different approaches and seasons.

Class	Winter				Summer				Dual-season			
	OBIA		Pixel		OBIA		Pixel		OBIA		Pixel	
	km²	%	km²	%	km²	%	km²	%	km²	%	km²	%
Water	464.14	39.7	432.42	37.0	435.20	37.2	400.95	34.3	451.96	38.7	406.44	34.8
Marsh	393.09	33.6	391.90	33.5	378.12	32.3	304.28	26.0	333.64	28.5	454.86	38.9
Dune	7.51	0.6	5.82	0.5	6.25	0.5	6.95	0.6	7.97	0.7	6.31	0.5
Trees and shrubs	21.91	1.9	15.04	1.3	19.66	1.7	41.84	3.6	14.60	1.2	12.45	1.1
Wet meadow	247.03	21.1	253.63	21.7	272.48	23.3	379.68	32.5	261.98	22.4	269.58	23.1
Crop	31.56	2.7	45.15	3.9	23.62	2.0	21.28	1.8	26.68	2.3	0.91	0.1
Bare soil	4	0.3	25.28	2.2	33.91	2.9	14.26	1.2	72.41	6.2	18.69	1.6
Total area	1169.24	100	1169.24	100	1169.24	100	1169.24	100	1169.24	100	1169.24	100
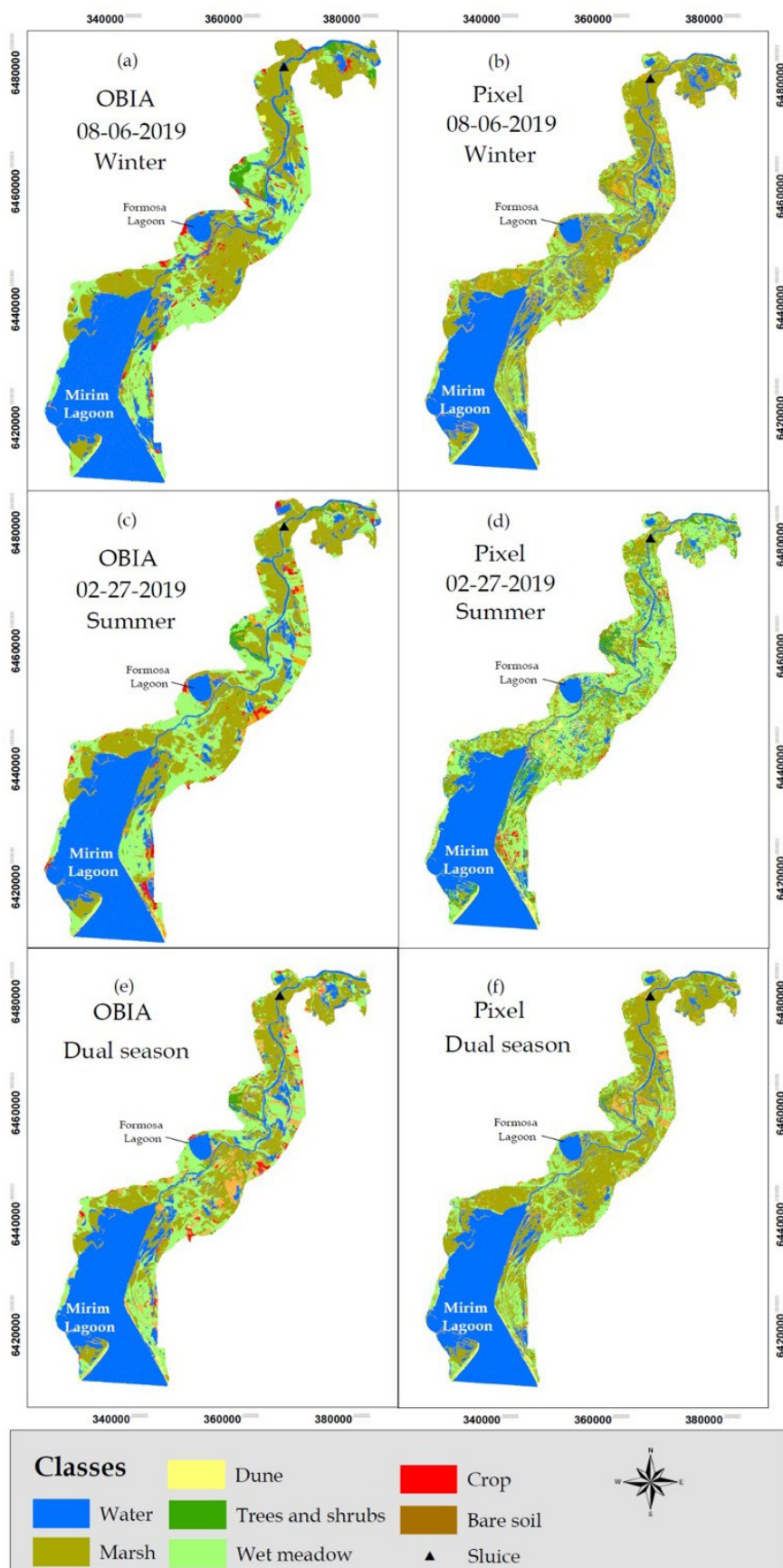
Figure 5. Dual-season classification using OBIA and pixel-based approach. (a) OBIA-based classification in winter; (b) pixel-based classification in winter; (c) OBIA-based classification in summer; (d) pixel-based classification in summer; (e) OBIA-based classification in dual season; (f) pixel-based classification in dual season.

Figure 6. Scirpus Giganteus Kunth (a); Wet meadow (b), São Gonçalo channel.
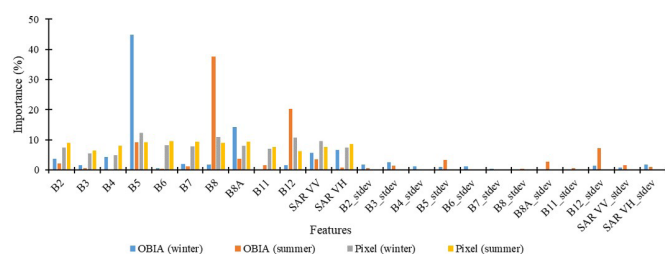
Figure 7. Importance of features (%) using OBIA and Pixel approaches in in different seasons.

The summer OBIA showed an accuracy of 0.82 and a kappa coefficient of 0.79. When the user's accuracy is less than the producer's accuracy, there is probably an overestimation of the classes.

For the winter image, the overall accuracy of the pixel-based approach was 9% lower compared to OBIA. The difference between the rankings is even greater when looking at the kappa coefficient, for the pixel-based approach (0.68) compared to OBIA (0.80). For summer the difference between the overall OBIA and pixel-based accuracy increases to 12% and for the kappa coefficient to 0.17, showing significant differences between different approaches and for different dates.

The OBIA and Pixel approaches and the Summer and Winter seasons showed variations in the importance of the models (Figure 7). In winter, band B5 was the most important (44.79%) in the OBIA approach and in the Pixel approach (12,36%). In summer, the most important band based on OBIA was B8 (37.54%), and based on pixels (summer) the most important was B6 (9.52%) and the lowest B12 (6.21%), with values very close to importance. For OBIA, the greatest importance occurred in the mean of the objects, and the standard deviation of the objects was not significant in the models.

DISCUSSION

This work aimed to compare OBIA and pixel-based approaches to classify a subtropical coastal wetland, taking into account summer and winter images. Our results show that OBIA was more than 80% accurate in classifying coastal wetlands in both seasons. The best accuracy for the pixel-based approach was 74%.

This can be explained by two reasons: i) OBIA's ability to incorporate the shape variable into the model, since rice is cultivated in plots; ii) in the pixel-based approach, rice growing areas can be more confused with swamp and wet meadow classes due to the moisture content of vegetation that influences the reflectance of optical images and the backscattering of SAR images.

The lower accuracy of the pixel-based classification may be associated with speckle noise which creates a salt and pepper effect in the images. In addition, pixel-based classification ignores contextual and topological information of images (Pande-Chhetri et al., 2017). OBIA avoids this problem, as long as the segmentation process is of a high standard (Whyte et al., 2018).

Positive results were obtained by Belloli et al. (2022) by integrating optical images and Sentinel-1 and 2A SAR, combined with OBIA and RF, to classify vegetation cover typologies in humid areas. The highest accuracies occurred in segmentations with lower similarity thresholds and with higher tree parameters and therefore more complex in RF. Soffianian et al. (2023) compared the performance of pixel- and object-based methods in Support Vector Machine (SVM) and Random Forest (RF) algorithms for mapping mangrove ecosystems with Sentinel-2. Pixel-based classifications were strongly influenced by the effect of salt and pepper noise. Object-based classifications, with higher kappa, performed better than pixel-based ones. According to these authors, landscape metrics showed that classification methods can be affected in quantifying area and size metrics.

The difference in accuracy between the two stations could be related to water level fluctuations. In winter, the period with the highest occurrence of flood pulses, there is a greater presence of water, easily classified with bands B8 and B12. One indicator for monitoring wetland functioning is the extent of flooding in the form of pulses. The characterization of these fluctuations is the basis for understanding temporal limnological changes (Robinson et al., 2015; Liu et al., 2017; Karim et al., 2020). In the summer (dryer period), these areas are covered by wet meadows, a class that presented low accuracy for the producer and for the user, mainly in the pixel-based approach due to the spectral similarity with swamps and rice cultivation (Mahdavi et al., 2019).

Our results highlight that object-based classification has greater potential for classifying wetlands than pixel-based methods using the same classification algorithm. Foody (2002) and Mui et al. (2015) recommend global accuracy for land use and land cover mapping of 85%.

However, global accuracy for classifying wetlands requires a review of these values, given the difficulties in classifying these environments. These difficulties are related to access to collect training and validation samples (Dronova, 2015), the spectral similarity between different types of wetlands (wet meadows, swamps and rice cultivation) (Amani et al., 2018), fluctuations in water level (Grimson et al., 2019). However, we understand that even in the face of these difficulties, we reached global accuracy values very close to those recommended by (Mui et al., 2015), (83% in winter and 82% in summer), highlighting the potential of OBIA for classification of wetlands.

The class with the largest area is water, as the limits of the SGC cover areas of the Mirim and Formosa lakes. The marshy areas cover approximately 40,000 ha and are mainly composed of *Scirpus giganteus Kunth* (Figure 7). When analyzing the dynamics of the vegetation in a swamp in southern Brazil, it was found that there are no significant differences in the reflectance of *Scirpus giganteus Kunth* during the year, given the high leaf turnover, with continuous growth and new green leaves, even during the months of winter (Guasselli, 2005; Pratolongo et al., 2005). We verified that the presence of the sluice did not change the distribution patterns of the species. The main effects of the blockade are observed, for example, in the water level oscillation (Duarte, 2013), in the water quality (Albertoni et al., 2017).

Wet meadow areas cover ~25,000 ha during the Winter, and ~27,000 ha in the Summer. For Ruiz et al. (2021) the optical characteristics, the red edge and the two short wavelength infrared bands contributed values greater than 6%, and that the integration of optical images and SAR, with GEOBIA and data mining, was successful in classification of wetland vegetation classes. We also found that percentage of the SGC are used for agricultural purposes, especially rice cultivation. According to Chatziantoniou et al. (2017) areas of rice crops can be easily identified by OBIA from the shape of the regular plots of these areas.

In relation to the most important features in OBIA, we highlight the Sentinel 2A bands B5, B8, B8A and B12, which had more than 10% of importance in the models. The B5 feature of Sentinel 2a had the greater general importance in OBIA winter (44.7%). This feature corresponds to the band Red Edge 1. The reflectance value in this range is related to biochemical parameters of vegetation (for example, chlorophyll content), biophysical parameters (for example, Leaf Area Index) and water deficit in vegetation biomass (Mahdavi et al., 2019).

The features B8 (near infrared) and B12 (shortwave infrared 2) stood out in the OBIA-based approach for the summer (37.5% and 20.3% of importance in the model, respectively). In B8 the incident radiation is reflected by the mesophilic cells, but is strongly absorbed by water with a low concentration of suspended sediments, accentuating the contrast between green vegetation and water in heterogeneous environments (Taddeo et al., 2019). B12 is sensitive to soil moisture and vegetation, helping to distinguish healthy moist vegetation from senescent parts of plants (Taddeo et al., 2019), which justify the importance of these features in the model.

The SAR bands provide valuable information on soil moisture conditions (Kasischke et al., 2008; Adeli et al., 2020), structure of vegetation (Furtado et al., 2016; Morandeira et al., 2016;

Simioni et al., 2019; Wang et al., 2023) and hydrology (Dabboor & Brisco, 2018; Mahdavi et al., 2019; Palomino-Ángel et al., 2019; Rapinel et al., 2020) of wetlands.

Salem & Hashemi-Beni (2022) compared flood classifications using linear, dual and full polarizations of SAR ensembles. The L band classification was the most accurate. By mapping flooded vegetation using Sentinel-1, C-band and ALOS-2/PALSAR-2, L-band, Plank et al. (2017) highlighted that the C band (Sentinel-1) is more suitable for water detection, while the L band (ALOS-2/PALSAR-2) is better for flooded vegetation.

However, our results demonstrated that the SAR VV and VH features did not show significant importance in the models. The SAR polarization with the greatest importance in the classifications was pixel-based SAR VV (winter) (9.6%), and the SAR VH feature in the pixel-based approach (summer) classification (8.6%).

CONCLUSION

This study aimed to mapping coastal wetlands, which provide important ecosystem services and serve as habitats for several species. We conclude that the object-based approach showed greater potential for mapping subtropical wetlands, with accuracy greater than 80%. Therefore, the use of OBIA has a higher potential to classify wetlands in comparison to pixel-based approaches.

Optical images showed greater importance for classifying wetlands considering both approaches (OBIA and pixel-based). The features that showed greater relevance were the B5 (Red Edge 1) and B8 (near infrared) of Sentinel 2a, highlighting the importance of multispectral images to classify wetlands. The OBIA dual-season classification increased kappa by up to 7% when compared to the OBIA single-season. Also, the pixel-based dual-season had a lower kappa than the OBIA single-season. Therefore, we conclude that the OBIA-based approach, even in single-season, is the method that has the greatest potential for mapping subtropical coastal wetlands.

For future work, it is suggested to apply other resources in the OBIA-based approach, such as the geometric characteristics of the images, vegetation indices and SAR images with HH and HV polarizations. This work was conducted in a coastal wetland in southern Brazil, but the object-based approach may have high potential for mapping other subtropical coastal wetlands around the globe, given its ability to incorporate features such as shape, texture, size, geometry, among others.

ACKNOWLEDGEMENTS

REFERENCES

Abdikan, S., Sanli, F. B., Ustuner, M., & Calò, F. (2016). Land cover mapping using Sentinel 1 SAR data. *The International Archives of the Photogrammetry, Remote Sensing and Spatial Information Sciences*, *757-761*, http://dx.doi.org/10.5194/isprsarchives-XLI-B7-757-2016.

Adeli, S., Salehi, B., Mahdianpari, M., Quackenbush, L. J., Brisco, B., Tamiminia, H., & Shaw, S. (2020). Wetland monitoring using SAR data: a meta-analysis and comprehensive review. *Remote Sensing*, *12*, 2190. http://dx.doi.org/10.3390/rs12142190.

Albertoni, E. F., Palma-Silva, C., Trindade, C. R., & Furlanetto, L. M. (2017). Water quality of the São Gonçalo channel, urban and agricultural water supply in southern Brazil. *Brazilian Journal of Water Resources*, *22*, e2. https://doi.org/10.1590/2318-0331.011716082

Amani, M., Salehi, B., Mahdavi, S., & Brisco, B. (2018). Spectral analysis of wetlands using multi-source optical satellite imagery. *ISPRS Journal of Photogrammetry and Remote Sensing*, *144*, 119-136. http://dx.doi.org/10.1016/j.isprsjprs.2018.07.005.

Belloli, T. F., Guasselli, L. A., Kuplich, T., Ruiz, L. F. C., & Simioni, J. P. D. (2022). Object-based classification of vegetation cover typologies in wetland, integrating optical images and SAR. *Revista Brasileira de Cartografia*, *74*, 1. http://dx.doi.org/10.14393/rbcv74n1-61277.

Bergamo, T. F., Ward, R. D., Joyce, C. B., Villoslada, M., & Sepp, K. (2022). Experimental climate change impacts on Baltic coastal wetland plant communities. *Scientific Reports*, *12*, 20362.

Berhane, T. M., Lane, C. R., Wu, Q., Anenkhonov, O. A., Chepinoga, V. V., Autrey, B. C., & Liu, H. (2018). Comparing pixel- and object-based approaches in effectively classifying wetland-dominated landscapes. *Remote Sensing*, *10*, http://dx.doi.org/10.3390/rs10010046.

Blaschke, T., Hay, G. J., Kelly, M., Lang, S., Hofmann, P., Addink, E., Queiroz Feitosa, R., van der Meer, F., van der Werff, H., van Coillie, F., & Tiede, D. (2014). Geographic object-based image analysis: towards a new paradigm. *ISPRS Journal of Photogrammetry and Remote Sensing*, *87*, 180-191. http://dx.doi.org/10.1016/j.isprsjprs.2013.09.014.

Breiman, L., Friedman, J., Stone, C. J., & Olshen, R. A. (1984). *Classification and regression trees*. Belmont: Wadsworth.

Burger, M. I. (2000). *Situação e ações prioritárias para a conservação de banhados e áreas úmidas costeiras*. Porto Alegre: FZB-RS.

Burns, M. D. M. (2010). *Consequências da barragem eclusa do Canal São Gonçalo para a ictiofauna do sistema Patos-Mirim* (Tese de doutorado). Universidade Federal do Rio Grande, Rio Grande. Retrieved in 2022, October 6, from https://ppgocbio.furg.br/dissertacoes-e-teses/61-publicacoes-de-2010/409-353tese-marcelo-dias-de-mattos-burns

Chatziantoniou, A., Psomiadis, E., & Petropoulos, G. (2017). Co-Orbital sentinel 1 and 2 for LULC mapping with emphasis on wetlands in a mediterranean setting based on machine learning. *Remote Sensing*, *9*, 1259. http://dx.doi.org/10.3390/rs9121259.

Clevers, J. G. P. W. (2015). Microwave radar and radiometric remote sensing. *International Journal of Applied Earth Observation and Geoinformation*, *34*, 264-265. http://dx.doi.org/10.1016/J.JAG.2014.08.003.

Collischonn, E. (2016). Entering the city of Pelotas to take its temperature. *Revista do Departamento de Geografia*, *Volume Especial*, 9-23.

Costa, M., Evans, T., & Silva, T. S. F. (2016). Remote sensing of wetland types: subtropical wetlands of southern hemisphere. In: C. M. Finlayson, M. Everard, K. Irvine, R. J. McInnes, B. A. Middleton, A. A. van Dam & N. C. Davidson (Eds.), *The wetland book* (pp. 1-6). Dordrecht: Springer. https://doi.org/10.1007/978-94-007-6172-8_307-2

Cunha, C. S., Guasselli, L. A., Belloli, T. F., & Korb, C. C. (2023). Classification of Potential Wetlands using the Random Forest in Google Earth Engine in Geomorphological Units - Rio Grande do Sul, Brazil. *Revista Brasileira de Cartografia*, *75*, http://dx.doi.org/10.14393/rbcv75n0a-69753.

Dabboor, M., & Brisco, B. (2018). Wetland monitoring and mapping using synthetic aperture radar. In D. Gokce (Ed.), *Wetlands management: assessing risk and sustainable solutions* (pp. 61-86). London: Intechopen. http://dx.doi.org/10.5772/intechopen.80224

Daí, X., Wan, R., Yang, G., Wang, X., Xu, L., Li, Y., & Li, B. (2019). Impact of seasonal water-level fluctuations on autumn vegetation in Poyang Lake wetland, China. *Frontiers of Earth Sciences*, *13*(2), 398-409. http://dx.doi.org/10.1007/s11707-018-0731-y.

Dronova, I. (2015). Object-based image analysis in wetland research: a review. *Remote Sensing*, *7*(5), 6380-6413. http://dx.doi.org/10.3390/rs70506380.

Duarte, R.F. (2013). *Monitoramento das áreas úmidas e inundadas adjacentes ao Canal São Gonçalo com uma série de imagens ERS-1/2 SAR e Envisat ASAR adquiridas entre 1992 e 2007* (Dissertação de mestrado). Universidade Federal do Rio Grande, Rio Grande.

Food and Agriculture Organization – FAO. (1972). *Desarrollo de la cuenca hidrográfica de la Lagoa Merin*. Montevideo: FAO.

Foody, G. M. (2002). Status of land cover classification accuracy assessment. *Remote Sensing of Environment*, *80*, 185-201. https://doi.org/10.1016/S0034-4257(01)00295-4.

Fu, B., Wang, Y., Campbell, A., Li, Y., Zhang, B., Yin, S., Xing, Z., & Jin, X. (2017). Comparison of object-based and pixel-based Random Forest algorithm for wetland vegetation mapping using high spatial resolution GF-1 and SAR data. *Ecological Indicators*, *73*, 105-117. http://dx.doi.org/10.1016/J.ECOLIND.2016.09.029.

Furtado, L. F. A., Silva, T. S. F., & Novo, E. M. L. M. (2016). Dual-season and full-polarimetric C band SAR assessment for vegetation mapping in the Amazon várzea wetlands. *Remote Sensing of Environment*, *174*, 212-222. http://dx.doi.org/10.1016/J.RSE.2015.12.013.

Gini, C. (1912). *Variabilita e mutabilita: contributo allo studio delle distribuzioni e delle relazioni statistiche*. Bologna: Archivio Cognetti.

Grimson, R., Gayol, M.P., Grimson, R., Morandeira, N.S., Gayol, M.P., & Kandus, P. (2019). Freshwater marsh classification in the Lower Paraná River floodplain: an object-based approach on multitemporal X-band COSMO- SkyMed data. *Journal of Applied Remote Sensing, 13*(1), 014531. http://dx.doi.org/10.1117/1.JRS.13.014531

Guasselli, L. A. (2005). *Dinâmica da vegetação no banhado do Taim, RS* (Tese de doutorado). Universidade Federal do Rio Grande do Sul, Rio Grande do Sul

Guo, M., Li, J., Sheng, C., Xu, J., & Wu, L. (2017). A review of wetland remote sensing. *Sensors (Switzerland), 17*, 1-36. http://dx.doi.org/10.3390/s17040777.

Happ, P. N., Feitosa, R. Q., Bentes, C., & Farias, R. (2013). Um algoritmo de segmentação por crescimento de regiões para GPUs. *Boletim de Ciências Geodésicas, 19*, 208-226. http://dx.doi.org/10.1590/S1982-21702013000200004

Instituto Nacional de Meteorologia – INMET. (2020). *Banco de dados meteorológicos*. Retrieved in 2022, September 2, from https://bdmep.inmet.gov.br/.

Instituto Rio Grandense do Arroz – IRGA. (2019). *Safra 2019/2020*. Retrieved in 2022, September 2, from https://irga.rs.gov.br/upload/arquivos/202007/23141617-produtividade-municipios-safra-19-20.pdf

Irgang, B. E., Gastal Junior, G., & De Senna, C. V. (1996). *Macrófitas aquáticas da planície costeira do RS*. Porto Alegre: CPG Botânica/UFRGS.

Jahncke, R., Leblon, B., Bush, P., & LaRocque, A. (2018). Mapping wetlands in Nova Scotia with multi-beam RADARSAT-2 Polarimetric SAR, optical satellite imagery, and Lidar data. *International Journal of Applied Earth Observation and Geoinformation, 68*, 139-156. http://dx.doi.org/10.1016/J.JAG.2018.01.012.

Junk, W. J., Piedade, M. T. F., Lourival, R., Wittmann, F., Kandus, P., Lacerda, L. D., Bozelli, R. L., Esteves, F. A., Nunes da Cunha, C., Maltchik, L., Schöngart, J., Schaeffer-Novelli, Y., & Agostinho, A. A. (2014). Brazilian wetlands: their definition, delineation, and classification for research, sustainable management, and protection. *Aquatic Conservation, 24*, 5-22. http://dx.doi.org/10.1002/aqc.2386.

Kandus, P., Minotti, P. G., Morandeira, N. S., Grimson, R., Trilla, G. G., González, E. B., Martín, L. S., & Gayol, M. P. (2018). Remote sensing of wetlands in South America: status and challenges. *International Journal of Remote Sensing, 39*, 993-1016. http://dx.doi.org/10.1080/01431161.2017.1395971.

Kaplan, G., & Avdan, U. (2018). Sentinel-2 pan sharpening? Comparative analysis. *Proceedings, 2*, 1-6. http://dx.doi.org/10.3390/ecrs-2-05158.

Kaplan, G., & Avdan, U. (2019). Evaluating the utilization of the red edge and radar bands from sentinel sensors for wetland classification. *Catena, 178*, 109-119. http://dx.doi.org/10.1016/J.CATENA.2019.03.011.

Karim, F., Marvanek, S., Merrin, L. E., Nielsen, D., Hughes, J., Stratford, D., & Pollino, C. (2020). Modelagem da conectividade de áreas úmidas induzidas por inundações e dos impactos das mudanças climáticas e das barragens. *Water (Basel), 12*(5), 1278. http://dx.doi.org/10.3390/w12051278.

Kasischke, E. S., Bourgeau-chavez, L. L., Rober, A. R., Wyatt, K. H., Waddington, J. M., & Turetsky, M. R. (2008). Effects of soil moisture and water depth on ERSSAR backscatter measurements from an Alaskan wetland complex. *Remote Sensing of Environment, 113*, 1868-1873. http://dx.doi.org/10.1016/j.rse.2009.04.006.

Lawrence, R. L., & Wright, A. (2001). Rule-based classification systems using Classification and Regression Tree (CART) analysis. *Photogrammetric Engineering and Remote Sensing, 67*, 1137-1142. http://dx.doi.org/10.1016/S0034-4257(01)00247-4.

Lázaro, W. L., Oliveira-Júnior, E. S. O., Silva, C. J., Castrillon, S. K. I., & Muniz, C. C. (2020). Climate change reflected in one of the largest wetlands in the world: an overview of the Northern Pantanal water regime. *Acta Limnologica Brasiliensia, 32*, e104.

Li, C. H., Xian, Y., Ye, C., Wang, Y. H., Wei, W., Xi, H. Y., & Zheng, B. H. (2019). Wetland ecosystem status and restoration using the Ecopath with Ecosim (EWE) model. *The Science of the Total Environment, 658*, 305-314. http://dx.doi.org/10.1016/j.scitotenv.2018.12.128.

Liu, Y., Chen, G., Hu, K., Shi, H., Huang, L., Chen, X., Lu, H., Zhao, S., & Chen, L. (2017). Biological responses to recent eutrophication and hydrologic changes in Xingyun Lake, southwest China. *Journal of Paleolimnology, 57*(4), 343-360. http://dx.doi.org/10.1007/s10933-017-9952-4.

Mahdavi, S., Salehi, B., Amani, M., Granger, J., Brisco, B., & Huang, W. (2019). A dynamic classification scheme for mapping spectrally similar classes: application to wetland classification. *International Journal of Applied Earth Observation and Geoinformation, 83*, 101914. http://dx.doi.org/10.1016/J.JAG.2019.101914.

Mahdianpari, M., Salehi, B., Mohammadimanesh, F., & Motagh, M. (2017). Random forest wetland classification using ALOS-2 L-band, RADARSAT-2 C-band, and TerraSAR-X imagery. *ISPRS Journal of Photogrammetry and Remote Sensing, 130*, 13-31. http://dx.doi.org/10.1016/j.isprsjprs.2017.05.010.

Maltchik, R. L., Guadagnin, A. S., & Stenert, D. L. (2004). Wetlands of Rio Grande do Sul, Brazil: a classification with emphasis on plant communities. *Acta Limnologica Brasiliensia, 16*, 137-151.

Mengue, P. M., Freitas, M. W. D., Silva, T. S., Fontana, D. C., & Scottá, F. C. (2020). LAND-USE and land-cover change processes in Pampa biome and relation with environmental and socioeconomic data. *Applied Geography (Sevenoaks, England), 125*, 102342. http://dx.doi.org/10.1016/j.apgeog.2020.102342.

Milien, E. J., Nunes, G. M., Pierre, G., Hamilton, S. K., & Cunha, C. N. (2023). Hydrological dynamics of the pantanal, a large tropical floodplain in Brazil, revealed by analysis of sentinel-2 satellite imagery. *Water (Basel)*, *15*(12), 2180. http://dx.doi.org/10.3390/w15122180.

Mitsch, W. J., & Gosselink, J. G. (2015). *Wetlands* (5th ed.). New Jersey: Wiley.

Mohammadimanesh, F., Salehi, B., Mahdianpari, M., Brisco, B., & Motagh, M. (2018). Multi-temporal, multi-frequency, and multi-polarization coherence and SAR backscatter analysis of wetlands. *ISPRS Journal of Photogrammetry and Remote Sensing*, *142*, 78-93. http://dx.doi.org/10.1016/j.isprsjprs.2018.05.009.

Morandeira, N., Grings, F., Facchinetti, C., & Kandus, P. (2016). Mapping plant functional types in floodplain wetlands: an analysis of C-Band polarimetric SAR data from RADARSAT-2. *Remote Sensing*, *8*, 174. http://dx.doi.org/10.3390/rs8030174.

Mui, A., He, Y., & Weng, Q. (2015). An object-based approach to delineate wetlands across landscapes of varied disturbance with high spatial resolution satellite imagery. *ISPRS Journal of Photogrammetry and Remote Sensing*, *109*, 30-46. http://dx.doi.org/10.1016/j.isprsjprs.2015.08.005.

Palomino-Ángel, S., Anaya-Acevedo, J. A., Simard, M., Liao, T. H., & Jaramillo, F. (2019). Analysis of floodplain dynamics in the Atrato River Colombia using SAR interferometry. *Water (Switzerland)*, *11*, http://dx.doi.org/10.3390/w11050875.

Pande-Chhetri, R., Abd-Elrahman, A., Liu, T., Morton, J., & Wilhelm, V. L. (2017). Object-based classification of wetland vegetation using very high-resolution unmanned air system imagery. *European Journal of Remote Sensing*, *50*, 564-576. http://dx.doi.org/10.1080/22797254.2017.1373602.

Plank, S., Jüssi, M., Martinis, S., & Twele, A. (2017). Combining polarimetric sentinel-1 and ALOS-2/PALSAR-2 imagery for mapping of flooded vegetation. In *International Geoscience and Remote Sensing Symposium*. New York: IEEE. http://dx.doi.org/10.1109/IGARSS.2017.8128303

Pontius, R. G., & Millones, M. (2011). Death to Kappa: birth of quantity disagreement and allocation disagreement for accuracy assessment. *International Journal of Remote Sensing*, *32*, 4407-4429. http://dx.doi.org/10.1080/01431161.2011.552923.

Pratolongo, P., Vicari, R., Kandus, P., & Malvárez, I. (2005). A new method for evaluating Net Aboveground Primary Production (NAPP) of Scirpus giganteus (Kunth). *Wetlands*, *25*(1), 228-232. http://dx.doi.org/10.1672/0277-5212(2005)025[0228:ANMFEN]2.0.CO;2.

Prentice, R. M., Peciña, M. V., Ward, R. D., Bergamo, T. F., Joyce, C. B., & Sepp, K. (2022). Machine Learning classification and accuracy assessment from high-resolution images of Coastal Wetlands. *Remote Sensing*, *13*, 3669. http://dx.doi.org/10.3390/rs13183669.

Prudente, V. H. R., Skakun, S., Oldoni, L. V., Xaud, H. A. M., Xaud, M. R., Adami, M., & Sanches, I. D. (2022). Multisensor approach to land use and land cover mapping in Brazilian Amazon. *ISPRS Journal of Photogrammetry and Remote Sensing*, *189*, 95-109.

Radam Brasil. (1986). *Levantamento dos recursos naturais*. Radam: Rio de Janeiro.

Ramachandran, C., Parappurathu, S., Gills, R., Anuja, A. R., Padua, S., Kumar, R. R., & Rajesh, N. (2023). Ecosystem services of coastal wetlands for climate change mitigation: an economic analysis of Pokkali and Kaipad-based rotational paddy farming systems in India. *Current Science*, *125*, 2. Retrieved in 2023, September 11, from https://www.currentscience.ac.in/Volumes/125/02/0156.pdf

Rapinel, S., Betbedera, J., Denizeb, J., Fabrea, E., Pottierb, E., & Hubert-Moy, L. (2020). SAR analysis of wetland ecosystems: effects of band frequency, polarization mode and acquisition dates. *ISPRS Journal of Photogrammetry and Remote Sensing*, *170*, 103-113. http://dx.doi.org/10.1016/j.isprsjprs.2020.10.007.

Rapinel, S., Panhelleux, L., Gayet, G., Vanacker, R., Lemercier, B., Laroche, B., Chambaud, F., Guelmami, A., & Hubert-Moy, L. (2023). National wetland mapping using remote-sensing-derived environmental variables, archive field data, and artificial intelligence. *Heliyon*, *9*(2), e13482. http://dx.doi.org/10.1016/j.heliyon.2023.e13482.

Robinson, S. J., Souter, N. J., Bean, N. G., Ross, J. V., Thompson, R. M., & Bjornsson, K. T. (2015). Statistical description of wetland hydrological connectivity to the River Murray in South Australia under both natural and regulated conditions. *Journal of Hydrology (Amsterdam)*, *531*, 929-939. http://dx.doi.org/10.1016/j.jhydrol.2015.10.006.

Rojas, O., Sotoa, E., Rojasb, C., & López, J. J. (2022). Assessment of the flood mitigation ecosystem service in a coastal wetland and potential impact of future urban development in Chile. *Habitat International*, *123*, 102554.

Ruiz, L. F. C. (2018). *GeoPatterns*. Retrieved in 2023, September 11, from https://github.com/RuizGeo/GeoPatterns1.0.

Ruiz, L. F. C., Guasselli, L. A., Simioni, J. P. D., Belloli, T. F., & Fernandes, P. C. B. (2021). Object-based classification of vegetation species in a subtropical wetland using Sentinel-1 and Sentinel-2A images. *Science of Remote Sensing*, *3*, 100017.

Salem, A., & Hashemi-Beni, L. (2022). Inundated vegetation mapping using SAR data: a comparison of polarization configurations of UAVSAR L-Band and sentinel C-Band. *Remote Sensing*, *14*(24), 6374. http://dx.doi.org/10.3390/rs14246374.

Serviço Geológico do Brasil - SGB. (2004). *Geologia e Recursos Minerais do Estado de Rio Grande do Sul - Escala 1:750.000*. Brasília: CPRM.

Simioni, J. P. D., Guasselli, L. A., Nascimento, V. F., Ruiz, L. C. F., & Belloli, T. F. (2019). Integration of multi sensor analysis and decision tree for evaluation of dual and quad Pol SAR in L and C bands applied for marsh delineation. *Environment, Development and Sustainability*, http://dx.doi.org/10.1007/s10668-019-00442-0.

Simon, A. L. H., & Silva, P. F. (2015). Análise geomorfológica da planície lagunar sob influência do canal São Gonçalo-Rio Grande do Sul-Brasil. *Geociências*, *34*, 749-767.

Şimşek, Ç. K., & Ödül, H. (2018). Investigation of the effects of wetlands on micro-climate. *Applied Geography (Sevenoaks, England)*, http://dx.doi.org/10.1016/j.apgeog.2018.05.018.

Sinthumule, N. I. (2021). An analysis of communities' attitudes towards wetlands and implications for sustainability. *Global Ecology and Conservation*, *27*, e01604.

Soffianian, A. R., Toosi, N. B., Asgarian, A., Regnauld, H., Fakheran, S., & Wasers, L. T. (2023). Evaluating resampled and fused Sentinel-2 data and machine-learning algorithms for mangrove mapping in the northern coast of Qeshm island, Iran. *Nature Conservation.*, *52*, 1-22. http://dx.doi.org/10.3897/natureconservation.52.89639.

Story, M., & Congalton, R. G. (1986). Remote sensing brief accuracy assessment: a user's perspective. *Photogrammetric Engineering and Remote Sensing*, *52*, 397-399.

Taddeo, S., Dronova, I., & Depsky, N. (2019). Spectral vegetation indices of wetland greenness: responses to vegetation structure, composition, and spatial distribution. *Remote Sensing of Environment*, *234*, http://dx.doi.org/10.1016/j.rse.2019.111467.

Terra, A. B. C., Florentino, L. A., & Landgraf, P. R. (2022). Wetlands in Brazil: classification, floristic composition and biological Nitrogen fixation. *Research Social Development*, *11*(2), e40911225787. http://dx.doi.org/10.33448/rsd-v11i2.25787.

Tian, L., Wu, X., Tao, Y., Li, M., Qian, C., Liao, L., & Fu, W. (2023). Review of remote sensing-based methods for forest aboveground biomass estimation: progress, challenges, and prospects. *Forests*, *14*(6), 1086. http://dx.doi.org/10.3390/f14061086.

Tran, T. V., Reef, R., & Zhu, X. (2022). A review of spectral indices for mangrove remote sensing. *Remote Sensing*, *14*(19), 4868. http://dx.doi.org/10.3390/rs14194868.

Vanderhoof, M. K., Alexander, L. C., & Todd, M. J. (2016). Temporal and spatial patterns of wetland extent influence variability of surface water connectivity in the Prairie Pothole Region, United States. *Landscape Ecology*, *31*, 805-824. http://dx.doi.org/10.1007/s10980-015-0290-5.

Waheed, T., Bonnell, R. B., Prasher, S. O., & Paulet, E. (2006). Measuring performance in precision agriculture: CART-A decision tree approach. *Agricultural Water Management*, *84*, 173-185. http://dx.doi.org/10.1016/j.agwat.2005.12.003.

Wang, C., Pavelsky, T. M., Kyzivat, E. D., Garcia-Tigreros, F., Podest, E., Yao, F., Yang, X., Zhang, S., Song, C., Langhorst, T., Dolan, W., Kurek, M. R., Harlan, M. E., Smith, L. C., Butman, D. E., Spencer, R. G. M., Gleason, C. J., Wickland, K. P., Striegl, R. G., & Peters, D. L. (2023). Quantification of wetland vegetation communities features with airborne AVIRIS-NG, UAVSAR, and UAV LiDAR data in Peace-Athabasca Delta. *Remote Sensing of Environment*, *294*, 113646. http://dx.doi.org/10.1016/j.rse.2023.113646.

Wang, Y., Yésou, H., Wang, Y., & Yésou, H. (2018). Remote sensing of floodpath lakes and wetlands: a challenging frontier in the monitoring of changing environments. *Remote Sensing*, *10*, 1955. http://dx.doi.org/10.3390/rs10121955.

Whyte, A., Ferentinos, K. P., & Petropoulos, G. P. (2018). A new synergistic approach for monitoring wetlands using Sentinels -1 and 2 data with object-based machine learning algorithms. *Environmental Modelling & Software*, *104*, 40-54. http://dx.doi.org/10.1016/j.envsoft.2018.01.023.

Zhang, Z., Jiang, W., Peng, K., Wu, Z., Ling, Z., & Li, Z. (2023). Assessment of the impact of wetland changes on carbon storage in coastal urban agglomerations from 1990 to 2035 insupport of SDG15.1. *The Science of the Total Environment*, *877*, 162824. http://dx.doi.org/10.1016/j.scitotenv.2023.162824.

Zheng, J., Hao, Y., Wang, Y., Zhou, S., Wu, W., Yuan, Q., Gao, Y., Guo, H., Cai, X., & Zhao, B. (2022). Coastal wetland vegetation classification using pixel-based, object-based and deep learning methods based on RGB-UAV. *Land (Basel)*, *11*, 2039. http://dx.doi.org/10.3390/land11112039.

Authors contributions

João Paulo Delapasse Simioni: Image processing and classification; field data collection; discussion of results; final draft of the text.

Laurindo Antonio Guasselli: Literature review; field data collection; preparation and discussion of results; correction of the text.

Editor-in-Chief: Adilson Pinheiro

Associated Editor: Ibraim Fantin da Cruz